



# Effect of the annealing atmosphere on the electrochemical properties of RuO<sub>2</sub> nano-oxides synthesized by the Instant Method



T. Audichon <sup>a,\*</sup>, B. Guenot <sup>a,b</sup>, S. Baranton <sup>a</sup>, M. Cretin <sup>b</sup>, C. Lamy <sup>b</sup>, C. Coutanceau <sup>a,\*</sup>

<sup>a</sup> Université de Poitiers, IC2MP, UMR CNRS 7285, "Catalysis and Non-Conventional Media" Group, 4 Rue Michel Brunet, TSA 51106, 86073 Poitiers Cedex 9, France

<sup>b</sup> Université de Montpellier, Institut Européen des Membranes, UMR ENSCM, UM, CNRS n° 5635, 2 Place Eugène Bataillon, CC047, 34095 Montpellier Cedex 5, France

## ARTICLE INFO

### Article history:

Received 18 April 2017

Received in revised form 13 June 2017

Accepted 26 June 2017

Available online 29 June 2017

### Keywords:

Annealing temperature/atmosphere

Oxygen evolution reaction

Ruthenium oxide

Water electrolysis

## ABSTRACT

Ruthenium oxide materials have been synthesized by an "Instant method" assisted by microwave irradiation. The "as-synthesized" material has been annealed at different temperatures from 200 °C to 450 °C, under different atmospheres, air and nitrogen. The different samples were characterized by X-ray diffraction, transmission electron microscopy and cyclic voltammetry (capacitance, charges involved, etc.). The physicochemical and electrochemical characterizations have evidenced that the main effect of the annealing atmosphere is the modification of the transition temperature from an amorphous hydrated phase to a crystalline phase of ruthenium oxide (ca. 300 °C under air and ca. 350 °C under inert atmosphere according to XRD measurement). The activity of the different catalysts towards the oxygen evolution reaction was evaluated by linear scan voltammetry. In the high overpotential region ( $E > 1.6$  V vs. RHE), higher catalytic activities were obtained after annealing at high temperatures, i.e. 400–450 °C, independently on the annealing atmosphere. In the low overpotential region ( $E < 1.5$  V vs. RHE), higher activity in terms of exchange current density  $j_0$  was obtained for hydrated ruthenium oxide compounds, which was explained by the ability of materials to oxidize water molecules trapped in the ruthenium oxide lattice.

© 2017 Elsevier B.V. All rights reserved.

## 1. Introduction

Our technological civilization needs more and more energy and since 1850 [1] the world consumption of fossil fuels as energy resources has increased drastically. But their reserves are limited and will be exhausted in a few decades. Moreover, their use contributes to increase the CO<sub>2</sub> emissions and further to lead to stronger greenhouse effect [2]. To overcome these energy and environmental issues, it is important to diversify the energy sources and to promote energy systems based on eco-friendly resources without emission of harmful by-products. But, most of renewable primary energy sources, such as hydroelectric, wind, solar and tidal powers, are intermittent. Although they have known very intense developments for the last decades, energy storage solutions have to be developed in parallel, either in chemical or electrochemical systems. Hydrogen is a very promising energy vector, particularly

to feed fuel cells, but it is necessary to produce clean hydrogen to develop and promote this energy vector for such applications.

Currently, only 4% of hydrogen is produced by water electrolysis against 96% by reforming of fossil fuels [3]. To produce clean hydrogen, the proton exchange membrane water electrolyzer (PEMWE) is a particularly suitable device, but it still remains an expensive system. It is known that the main efficiency loss in such electrochemical systems is due to the oxygen evolution reaction (OER) at the anode which occurs at high overpotentials leading to high cell voltages, i.e. high energy consumption, whereas the hydrogen evolution reaction (HER) takes place at the cathode with negligible overpotentials.

Presently, higher efficiency for the OER is obtained in acidic media with anode catalysts composed of noble metal oxides. Ruthenium oxide-based materials are known to be amongst the most active electrocatalysts for the OER, also displaying low resistivity, high thermal and chemical stabilities, and high electronic conduction resulting from their rutile crystallographic structure [4,5]. However, their surface properties as well as their electrochemical behavior (electrocatalytic activity, selectivity, and stability) are known to depend greatly on the synthesis route. Fundamental investigations and extensive researches focused on their

\* Corresponding authors.

E-mail addresses: [thomas.audichon@univ-poitiers.fr](mailto:thomas.audichon@univ-poitiers.fr) (T. Audichon), [christophe.coutanceau@univ-poitiers.fr](mailto:christophe.coutanceau@univ-poitiers.fr) (C. Coutanceau).

fabrication, as bulk oxides [6], nano-oxides [7,8] and supported nano-oxides [9,10] using different chemical or physical methods were reported. The main challenge has remained the improvement of the long-term stability and the decrease of noble metal oxide loading in electrodes in order to minimize the cost without affecting the catalytic properties. The catalyst dispersion on high surface area electron conductive supports with high corrosion resistance, such as Sb-doped SnO<sub>2</sub> (ATO) [11,12], titanium sub-oxides (TiO<sub>x</sub>) [13], titanium carbides (TiC) [14], titanium nitrides (TiN) [15], titanium carbonitrides (TiCN) [15], etc., seems to be a promising way to reach these objectives. However, the synthesis of noble metal oxide particles generally requires a heat treatment step at high temperatures either under oxygen-containing atmospheres [11–13] or under inert atmospheres [14–16] depending on the support used. Indeed, TiC, TiN and TiCN supports are prone to a strong oxidation in air for temperatures higher than 300 °C [17–19] and generally, the catalyst deposition on such supports is performed via a thermal treatment under inert atmosphere leading to noble metals under metallic state [14–16]. Therefore, the comparison of the electrochemical behavior of the catalysts is made difficult due to strong differences in structure and compositions. This could be avoided by developing a synthesis method of metal oxide catalysts under inert atmosphere, which could allow protecting the support from oxidation during the thermal treatment step.

The present study is devoted to evaluate the effect of environment, air and inert gas atmospheres, in the heat treatment step on the morphology, structure and electrochemical properties of RuO<sub>2</sub> nanoparticles synthesized by the “Instant method” assisted by microwave irradiation [20]. The as-prepared and heat treated RuO<sub>2</sub> materials have been characterized by *in situ* X-ray diffraction (XRD) under controlled atmospheres and temperatures and by transmission electron microscopy (TEM). Their electrochemical properties (capacitance and electrocatalytic activity towards the oxygen evolution reaction) were investigated by cyclic voltammetry and linear potential scan measurements. The performances of non-supported particles prepared under inert atmosphere have been compared to those with non-supported particles prepared under air atmosphere, in order to determine the feasibility of a one-pot synthesis of noble metal oxide particles dispersed on new high corrosion-resistive electron conducting supports, such as titanium carbides, titanium nitrides and titanium carbonitrides.

## 2. Experimental

All chemical reagents were analytical grade and used without further purification. Ruthenium (III) chloride hydrate (RuCl<sub>3</sub>, xH<sub>2</sub>O, 99.99% metal basis) was purchased from Alfa Aesar. Lithium carbonate (Li<sub>2</sub>CO<sub>3</sub> > 99%) and Nafion® solution (5 wt% in aliphatic alcohol) were obtained from Sigma Aldrich.

### 2.1. Synthesis of ruthenium oxide nanoparticles

Electrocatalysts were synthesized using the “Instant Method” presented in a previous work [20]. First, desired amounts of RuCl<sub>3</sub>, xH<sub>2</sub>O and Li<sub>2</sub>CO<sub>3</sub> were separately dissolved in 20 mL of ultrapure water (MilliQ Millipore, 18.2 MΩ cm). Both solutions were sonicated for homogenization until translucent solutions were obtained (approximately 30 min). Then, the aqueous RuCl<sub>3</sub>, xH<sub>2</sub>O solution was added dropwise to the aqueous Li<sub>2</sub>CO<sub>3</sub> solution, under stirring at 500 rpm. The total mixture volume was adjusted to 50 mL in order to obtain concentrations of 0.01 mol L<sup>-1</sup> and 0.04 mol L<sup>-1</sup> for RuCl<sub>3</sub>, xH<sub>2</sub>O and Li<sub>2</sub>CO<sub>3</sub>, respectively. The mixture was sonicated for 30 min until a black solution was obtained. The pH value of the mixture was 9.5 ± 0.5, which is consistent with the basicity induced by the carbonate species. The reactor was equipped with

a cooler and placed in a microwave oven MARS 5 (CEM Corporation). The temperature of the mixture was increased up to 60 °C in less than 2 min (microwave power of 400 W) and kept for 20 min. After the solution has cooled down to room temperature, 50 mL of a water-ethanol mixture (1:1 v/v) was added in order to promote the particles decantation. Then the oxide nanoparticles were separated from solution by centrifugation at 15,000 rpm at 25 °C. The product was thoroughly washed with a water-ethanol mixture (1:1 v/v) until free of chloride and then dried at 80 °C overnight. The as-synthesized oxide material was designated as IM-80.

Samples of the IM-80 powder were annealed at different temperatures between 200 °C and 450 °C under air or nitrogen atmospheres with a heating rate of 3 °C min<sup>-1</sup> and the annealing temperature was held for 1 h. The materials obtained were referred to as IM-X-At, where X and At are the annealing temperature (between 200 °C and 450 °C) and the atmosphere (Air or N<sub>2</sub>), respectively. The sample labelling method was used for all synthesized materials, as the following examples IM-400-Air and IM-400-N<sub>2</sub>.

### 2.2. Electrochemical measurements

The electrochemical measurements were carried out in a standard three-electrode electrochemical cell at 20 °C. A reversible hydrogen electrode (RHE) and a glassy carbon slab were used as reference and counter electrodes, respectively. The RHE was connected to the cell via a Luggin capillary. The 0.5 M H<sub>2</sub>SO<sub>4</sub> (Merck, Suprapur) aqueous electrolyte was prepared with ultrapure water (MilliQ Millipore, 18.2 MΩ cm). A gold plate of 0.4 cm<sup>2</sup> geometric surface area was used as the working electrode. Before each experiment, the electrolyte was purged by bubbling ultra-pure nitrogen (U quality from L'Air Liquide) for 15 min and the nitrogen atmosphere was maintained in the electrochemical cell during the experiment. In order to check the cleanliness of the gold working electrode and of the cell, cyclic voltammograms were recorded in the supporting electrolyte prior to each measurement. The potential-current density curves were recorded using a Model 362 Scanning Potentiostat from Princeton Applied Research connected to a computer. Catalytic inks were prepared by mixing a suspension consisting of 10.8 mg of metal oxides in 3 mL of ultrapure water. For each electrochemical experiment, the anode was prepared by depositing 11.4 μL of the catalytic ink onto each face of the gold plate, which corresponded to a total loading of 0.2 mg of catalyst per cm<sup>2</sup>. The ink was dried under a slow nitrogen flow (U quality) and then 4 μL of a Nafion® solution, consisting in Nafion® (5 wt% in aliphatic alcohol from Aldrich) dispersed in ultrapure water with a mass concentration of 2 g<sub>Nafion</sub> L<sup>-1</sup>, was deposited on the catalytic layer, leading to ca. 17 wt% Nafion® loading.

### 2.3. Physical and physicochemical characterizations

*In situ* X-ray diffraction (XRD) patterns were recorded on a X-ray diffractometer (Bruker, D 8 Advance) with a copper target ( $K_{\alpha} = 1.5405 \text{ \AA}$ ) powered at 40 kV and 40 mA. The analysis was performed by heating the sample from room temperature up to 450 °C, with a ramp of 5 °C min<sup>-1</sup> under air or inert atmosphere (helium). The measurements were carried out in the 2θ range from 20° to 100° in step mode of 0.06° and a fixed acquisition time of 1 s step<sup>-1</sup>.

The morphology of the materials was examined by transmission electron microscopy (TEM). TEM images were acquired with a JEOL 2100UHR (200 kV) electron microscope equipped with a LaB<sub>6</sub> filament. TEM samples were prepared by depositing a drop of a suspension of IM-X-At in ethanol on a copper grid and by evaporating the solution under open atmosphere.

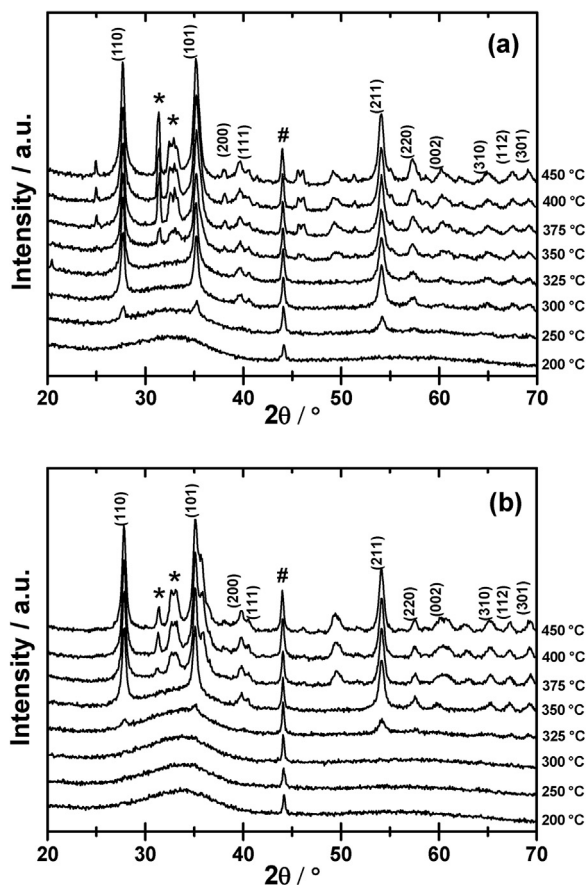


**Fig. 1.** *In situ* XRD patterns recorded on an IM-80 sample during annealing at different temperatures (a) under air atmosphere and (b) under inert atmosphere (He). # Kanthal sample holder; \* Lithium carbonate ( $\text{Li}_2\text{CO}_3$ ); the characteristic peaks of  $\text{RuO}_2$  were assigned from JCPDS 88-322 file.

### 3. Results and discussions

#### 3.1. Physicochemical characterizations

XRD patterns were recorded *in situ* in order to determine the nature and the crystallinity of the samples as a function of the annealing temperature and atmosphere (Fig. 1a and b, for annealing treatments under air and inert atmosphere, respectively). For both atmospheres, well defined diffraction peaks appear when increasing the annealing temperature. The most intense peaks of ruthenium dioxide rutile structure at  $2\theta = 28^\circ$ ,  $35^\circ$  and  $54^\circ$  become clearly distinguishable starting from  $250^\circ\text{C}$  under air against  $325^\circ\text{C}$  under inert atmosphere. For lower annealing temperatures, X-ray diffraction patterns do not present well defined peaks, only a broad peak at  $34^\circ$  is visible, which reveals that the  $\text{RuO}_2$  materials are amorphous or poorly crystalline. When the temperature is raised above  $300^\circ\text{C}$  under air and  $350^\circ\text{C}$  under inert atmosphere, characteristic diffraction peaks appear on the diffraction patterns, which, based on JCPDS database, could be attributed to reflection plans of the  $\text{RuO}_2$  rutile structure. The presence of well-defined peaks indicates a high crystallinity of ruthenium oxide in the samples; however some extra peaks appear in the  $30^\circ$ – $34^\circ$   $2\theta$  range under air and inert atmosphere for temperatures higher than  $350^\circ\text{C}$  and  $375^\circ\text{C}$ , respectively. Their presences could be attributed to traces of lithium carbonate not eliminated during the cleaning steps of the synthesis. The low intensity and the broadness of these peaks could indicate that the  $\text{Li}_2\text{CO}_3$  forms a thin layer on the surface of the  $\text{RuO}_2$  particles, which is difficult to eliminate by centrifugation. However, the presence  $\text{Li}_2\text{CO}_3$  on the oxide surface should

**Table 1**

Mean crystallite sizes of  $\text{RuO}_2$  materials synthesized by the "Instant Method" after annealing at different temperatures under air and inert atmospheres.

$T/\text{°C}$	Crystallite size/nm	
	Air atmosphere	Inert atmosphere
250	16.2	–
300	17.2	–
325	18.0	–
350	18.1	16.4
375	18.1	16.8
400	18.2	18.3
450	18.2	18.2

not affect their catalysts properties, since it will be dissolved in water during the elaboration of the electrocatalytic ink or in the electrolytic solution. As often described in the literature [21–23], when the annealing treatment is carried out under air atmosphere, crystalline ruthenium oxides are obtained from  $250^\circ\text{C}$ . By comparison, under inert atmosphere, the crystallinity appears for higher temperatures, although the nature of the as-synthesized material before heat treatment is the same for each annealing procedure. The presence of oxygen in annealing atmosphere during the heat treatment seems thus to promote the formation of oxide at a lower temperature whereas its absence tends to delay the formation of crystalline materials.

The average crystallite sizes of crystalline samples have been calculated using the Scherrer equation and are summarized in Table 1. The full width at half-maximum (fwhm) of the (110) diffraction peak located at  $27^\circ$  was used for the determination of the average mean crystallite size. Under air atmosphere, the mean crystallite size increases from 16.2 nm at  $250^\circ\text{C}$  up to 18.0 nm at  $325^\circ\text{C}$ , and remains constant for higher annealing temperatures. The same increase in mean crystallite size is observed under inert atmosphere, from 16.4 nm up to 18.3 nm, but over a range of higher temperatures, from  $350^\circ\text{C}$  to  $400^\circ\text{C}$ . Regardless on the annealing atmosphere, the lower mean crystallite size value of crystalline materials is ca. 16 nm and the higher mean crystallite size value at high annealing temperatures reaches ca. 18 nm in both cases. The microstructure of the final material seems not to depend on the heat treatment atmosphere but to be only correlated to the structure of the ruthenium hydroxide precursor.

TEM measurements were performed to analyse the morphology and the particles size changes of the synthesized materials as a function of the annealing atmosphere and temperature. Generally speaking, the global morphology of the samples is quite similar to what was observed by other authors using different routes for the synthesis of non-supported ruthenium oxides particles [8,24,25]. The particles are aggregated and the particle size distribution seems to be large, but the apparent mean particle sizes are always below 30 nm.

In the case of annealing under air atmosphere, the material obtained at  $300^\circ\text{C}$  shows aggregated amorphous particles (Fig. 2a). When the annealing temperature is increased, the particles appear better defined and present crystalline aspects (Fig. 2b–d), which is in agreement with XRD results. For the IM-450-Air sample, very well-defined particles, strongly aggregated, with a cuboid shape are obtained at  $450^\circ\text{C}$  (Fig. 2d).

In the case of annealing under inert atmosphere, the material obtained at  $300^\circ\text{C}$  (Fig. 2e) has not the same aspect as those obtained with heat treatment under air atmosphere. Although the material seems to present an amorphous aspect, it is not composed of amorphous particles, but rather constituted of very small crystallites having a few nanometer size. Same structures were obtained by Chang et al. [26] from a hydrothermal synthesis method, and where attributed to hydrated ruthenium oxides particles ( $\text{RuO}_2 \cdot x\text{H}_2\text{O}$ ) or to small agglomerates of hydroxide ruthenium species.

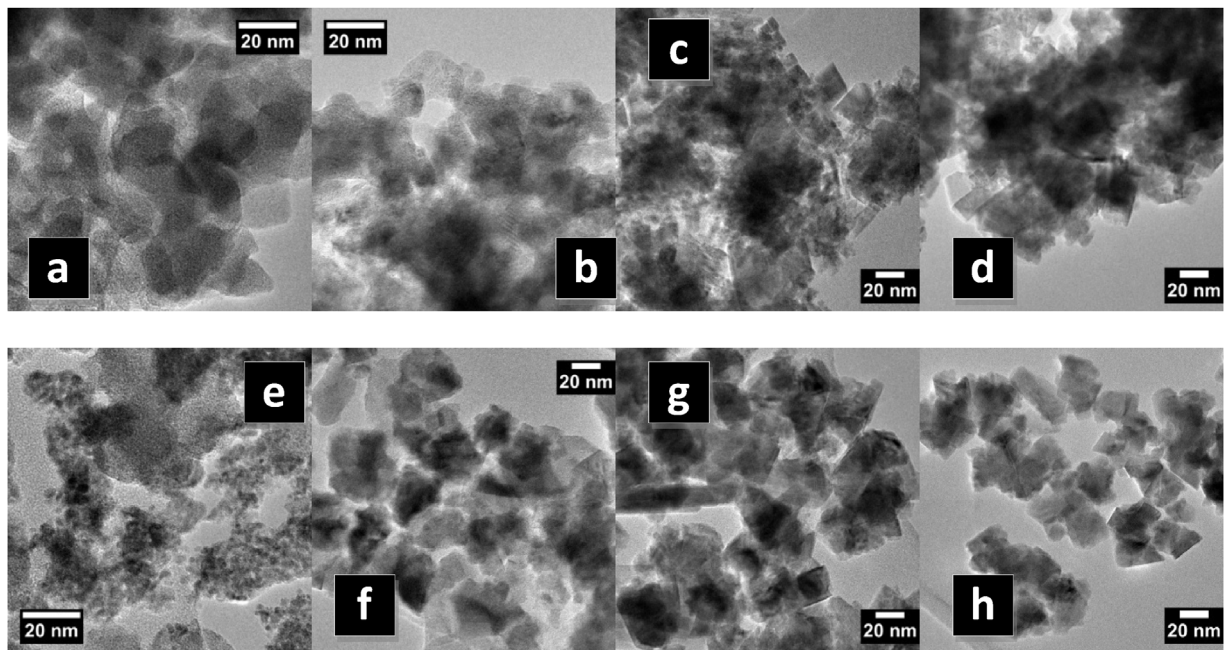


**Fig. 2.** TEM images of IM-X-At materials obtained after annealing (a–d) under air atmosphere and (e–h) under nitrogen atmosphere, at (a, e) 300 °C, (b, f) 350 °C, (c, g) 400 °C and (d, h) 450 °C.

At 350 °C, the ruthenium hydroxide species seem to sinter, forming bigger particles (Fig. 2f) and for higher temperatures, the particles become better defined and more and more shaped and their crystallinity increases. Comparison of TEM images in Fig. 2d (sample treated at 450 °C under air) and Fig. 2h (sample annealed at 450 °C under nitrogen) indicates a higher particle agglomeration for the sample treated under air than for the sample annealed under nitrogen. This behaviour, which is not an artefact of a single observation, was observed every time. It seems that the annealing treatment under inert atmosphere modifies the particle surface in a way that their trend to aggregate is limited. This property could be interesting in the objective of well dispersing catalysts on a corrosion-resistant electron-conducting support in order to obtain high active surface areas.

### 3.2. Electrochemical characterizations

In order to determine the impact of the annealing atmosphere on the structure of the synthesized oxides, cyclic voltammograms were recorded at 20 mV s<sup>-1</sup> in the H<sub>2</sub>SO<sub>4</sub> supporting electrolyte in the potential range from 0.05 to 1.4 V vs. RHE (Fig. 3a and b). All the current densities were normalized with the geometric surface area of the working electrode. Globally, the behaviors under potential control of the different materials are almost similar. However, some differences can be observed by comparing the cyclic voltammogram, which can be correlated to the amorphous or crystalline structure of the particles as previously observed by XRD and TEM depending on the annealing atmospheres and temperatures. The IM-300-Air sample (Fig. 3a) gives a CV with a shape characteristic of that of a hydrated or amorphous ruthenium oxide [27]. Very low current densities are observed below 0.3 V vs. RHE, which is attributed to low capacitive properties of the oxide material. In this case, water molecules present in the crystalline structure could act as a barrier for the electrons hopping process, limiting the values of the current densities. Between 0.6 and 0.9 V vs. RHE the voltammogram displays large quasi-reversible peaks which, according to the literature, are due to the overlapping of the redox transitions Ru(III)/Ru(IV) and Ru(IV)/Ru(VI) [24,28]. At last, the anodic

peak observed at 1.2 V vs. RHE is attributed to the redox transition Ru(VI)/Ru(VIII) [29]. All these redox transitions involve proton transfer only on the material surface which is a faradaic process leading to the formation of hydroxide surface species [30]. For the IM-325-Air sample, the CV displays the same shape, however the current densities are lower which reveals that the material is still amorphous but that the particles are partially dehydrated leading to a decrease of their capacitive properties. After annealing at 350 °C and 375 °C, both samples lead to very similar voltammograms in terms of shape and current densities achieved over the whole potential range of experiments, but are different from those obtained on samples annealed at lower temperatures. Although all redox transitions are still clearly visible and located at the same potentials, an additional non-reversible cathodic peak appears between 0.3 and 0.05 V vs. RHE. This peak is commonly attributed to the atomic hydrogen adsorption or insertion into the oxide lattice and is directly linked to the crystalline nature of the oxide material. Although the crystalline nature of the sample was observed from 250 °C on XRD patterns, this voltammetric peak is only observed on sample annealed at temperatures higher than 350 °C. This indicates that between 300 °C and 350 °C, the particles are crystalline (according to XRD measurements) but hydrated (according to electrochemical measurements), which could confer good capacitive and OER properties to such oxide materials, whereas materials annealed at higher temperatures are crystalline but dehydrated. At last, samples annealed at 400 °C and 450 °C present CVs whose shapes do not change and are characteristic of crystalline RuO<sub>2</sub>, whereas the current density values decrease indicating the increase of the crystallinity and the decrease of the oxide surface area in contact with the electrolyte.

The CVs of IM-300-N<sub>2</sub> and IM-325-N<sub>2</sub> (Fig. 3b) present similar shapes and current densities over the whole potential range. These voltammograms are characteristic of amorphous or hydrated RuO<sub>2</sub> particles and reveal only capacitive properties of oxide material with the redox transitions Ru(III)/Ru(IV), Ru(IV)/Ru(VI) and Ru(VI)/Ru(VIII) involving the formation of surface hydroxides as previously described. Thus, the atmosphere has no effect on the material structure for annealing temperatures of 300 and 325 °C.

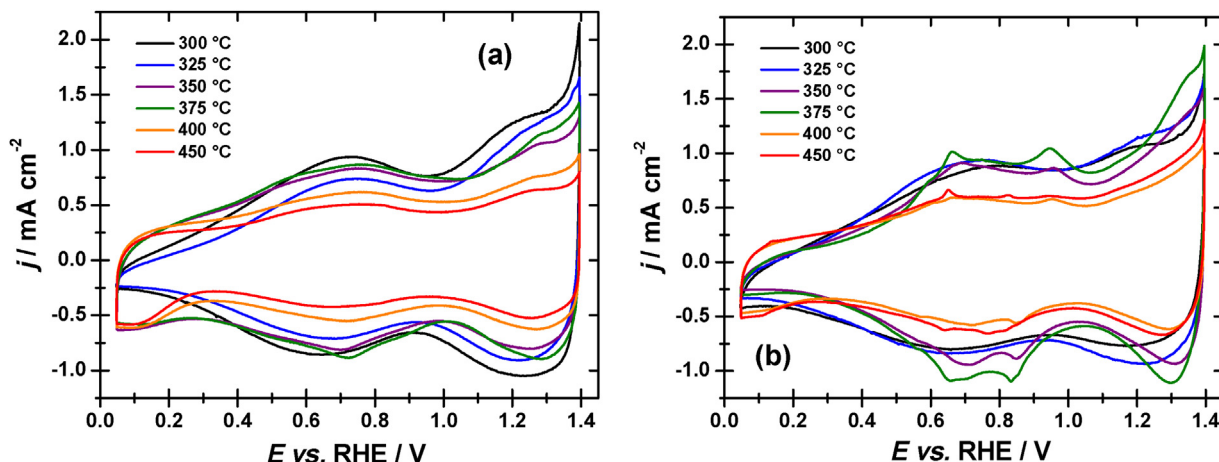


**Fig. 3.** Voltammograms of IM-X-At samples obtained in  $0.5 \text{ mol L}^{-1} \text{H}_2\text{SO}_4$  electrolyte recorded at  $20 \text{ mV s}^{-1}$  for each annealing temperature (a) under air atmosphere and (b) under nitrogen atmosphere.

However, for the samples annealed under inert atmosphere, the dehydration process seems to not occur at these temperatures since no decrease of current densities is observed. Conversely to the case of samples annealed under air at  $350^\circ\text{C}$  and  $375^\circ\text{C}$ , the CVs recorded on IM-350-N<sub>2</sub> and IM-375-N<sub>2</sub> do not present any cathodic peak at potentials lower than  $0.3 \text{ V}$  vs. RHE, which is an indication of the low crystallinity of these oxide materials. Although the crystallinity of the IM-350-N<sub>2</sub> and IM-375-N<sub>2</sub> samples was demonstrated by XRD measurements, the non-reversible cathodic peak between  $0.3$  and  $0.05 \text{ V}$  vs. RHE is not observed on these CVs. The presence of water in the crystalline structure may avoid the diffusion of hydrogen, and further its insertion in the oxide lattices.

The dehydration of the ruthenium oxide particles occurs at higher temperatures under inert atmosphere than under air. In the annealing temperature range from  $350^\circ\text{C}$  to  $450^\circ\text{C}$  under an inert atmosphere, two anodic peaks at  $0.65 \text{ V}$  and  $0.95 \text{ V}$  vs. RHE (and two cathodic peaks at  $0.85$  and  $0.65 \text{ V}$  vs. RHE, respectively) superimpose to the broad peaks observed for lower temperatures. They can be attributed to the redox transition Ru(III)/Ru(IV) and to the redox transition Ru(IV)/Ru(VI), respectively. Their appearance could indicate the formation of preferential crystalline orientations after annealing under inert atmosphere, increasing the number of surface active sites for surface hydroxide formation. Such two pairs of anodic/cathodic peaks have already been observed on RuO<sub>2</sub>(110) and RuO<sub>2</sub>(111) single crystals [31], although not resolved. The small shoulder in the anodic scan at  $1.3 \text{ V}$  vs. RHE corresponds to the redox transition Ru(VI)/Ru(VIII) [29]. When increasing the annealing temperature up to  $400^\circ\text{C}$  and  $450^\circ\text{C}$ , the current densities decrease, indicating an increase of the crystallinity of materials. Simultaneously, cathodic peaks characteristic of the hydrogen absorption in the oxide lattice appear. Moreover, the peaks correlated to the redox transitions are always present but less well defined.

Fig. 4 compares the CV recorded on samples annealed at the same temperature under both atmospheres. The current densities recorded over the whole potential range are very close whatever the annealing temperature and atmosphere, which suggests that the annealing atmosphere has no significant effect on the particle structure. The CVs recorded on catalysts annealed at low ( $300^\circ\text{C}$  and  $325^\circ\text{C}$ ) and high ( $400^\circ\text{C}$  and  $450^\circ\text{C}$ ) temperatures under both atmospheres are indeed very similar in shapes, respectively, and further the processes occurring at the surface of the electrocatalysts should also be the same. Conversely, differences in CV shapes are observed for samples annealed at intermediate temperatures, indicating that the morphological and crystalline changes are not

**Table 2**

Specific capacitances measured at different scan rates in  $0.5 \text{ M H}_2\text{SO}_4$  of RuO<sub>2</sub> materials annealed at different temperatures between  $300^\circ\text{C}$  and  $450^\circ\text{C}$  under ambient air or nitrogen atmosphere.

Scan rate	Specific capacitance ( $\text{F g}^{-1}$ )				$C(2 \text{ mV s}^{-1})/C(200 \text{ mV s}^{-1})$			
	2 $\text{mV s}^{-1}$		20 $\text{mV s}^{-1}$		200 $\text{mV s}^{-1}$		Air	N <sub>2</sub>
	Air	N <sub>2</sub>	Air	N <sub>2</sub>	Air	N <sub>2</sub>		
IM-300	n.d.	200.8	196.9	185.2	n.d.	155.5	n.d.	1.29
IM-325	166.7	213.3	159.0	196.1	140.4	170.7	1.19	1.25
IM-350	175.7	182.8	163.5	172.8	144.8	145.7	1.19	1.26
IM-375	197.1	194.7	182.8	189.5	163.3	159.1	1.21	1.22
IM-400	134.1	130.7	127.3	122.1	118.4	110.0	1.16	1.19
IM-450	109.4	143.6	98.6	133.8	86.7	120.7	1.26	1.19

n.d.: not determined.

only dependent on the annealing temperature, but also depend on the annealing atmosphere.

Elsewhere, it has been reported that the currents densities in the CV are the sum of a capacitive contribution (charge accumulation at the electrode/electrolyte interface) and a faradaic contribution (surface hydroxide formation) [32]. All these electrochemical processes occur at the electrocatalyst/electrolyte interface, hence the specific capacitance values for the RuO<sub>2</sub> materials were determined by integrating the anodic or the cathodic intensities,  $I(E)$ , of the linear scan voltammograms and by averaging the obtained values, using Eq. (1). The capacitance values  $C$  are expressed in  $\text{F g}^{-1}$ .

$$C = \frac{\Delta Q}{m \times \Delta E} = \frac{1}{v \times m \times (E_2 - E_1)} \int_{E_1}^{E_2} I(E) dE \quad (1)$$

where  $v$  is the scan rate ( $\text{V s}^{-1}$ ),  $m$  is the mass in gram of RuO<sub>2</sub> material deposited on the working electrode,  $E_1$  and  $E_2$  are the lower and upper potential limits of the scan for the integration process ( $0.3 \text{ V}$  and  $1.2 \text{ V}$  vs. RHE, respectively) and  $I(E)$  is the current at electrode potential  $E$ .

The specific capacitance values obtained at 2, 20 and  $200 \text{ mV s}^{-1}$  on the different materials are summarized in Table 2. Whatever the atmosphere, the specific capacitance values decrease when increasing the scan rate, which is correlated to the diffusion of the electro-reactive species from the electrolyte to the active sites inside the bulk of materials. For the materials prepared by annealing under air atmosphere, the trend for the specific capacitance values is to increase with the increase of annealing temperature for materials annealed between  $325^\circ\text{C}$  and  $375^\circ\text{C}$ , and then to decrease for

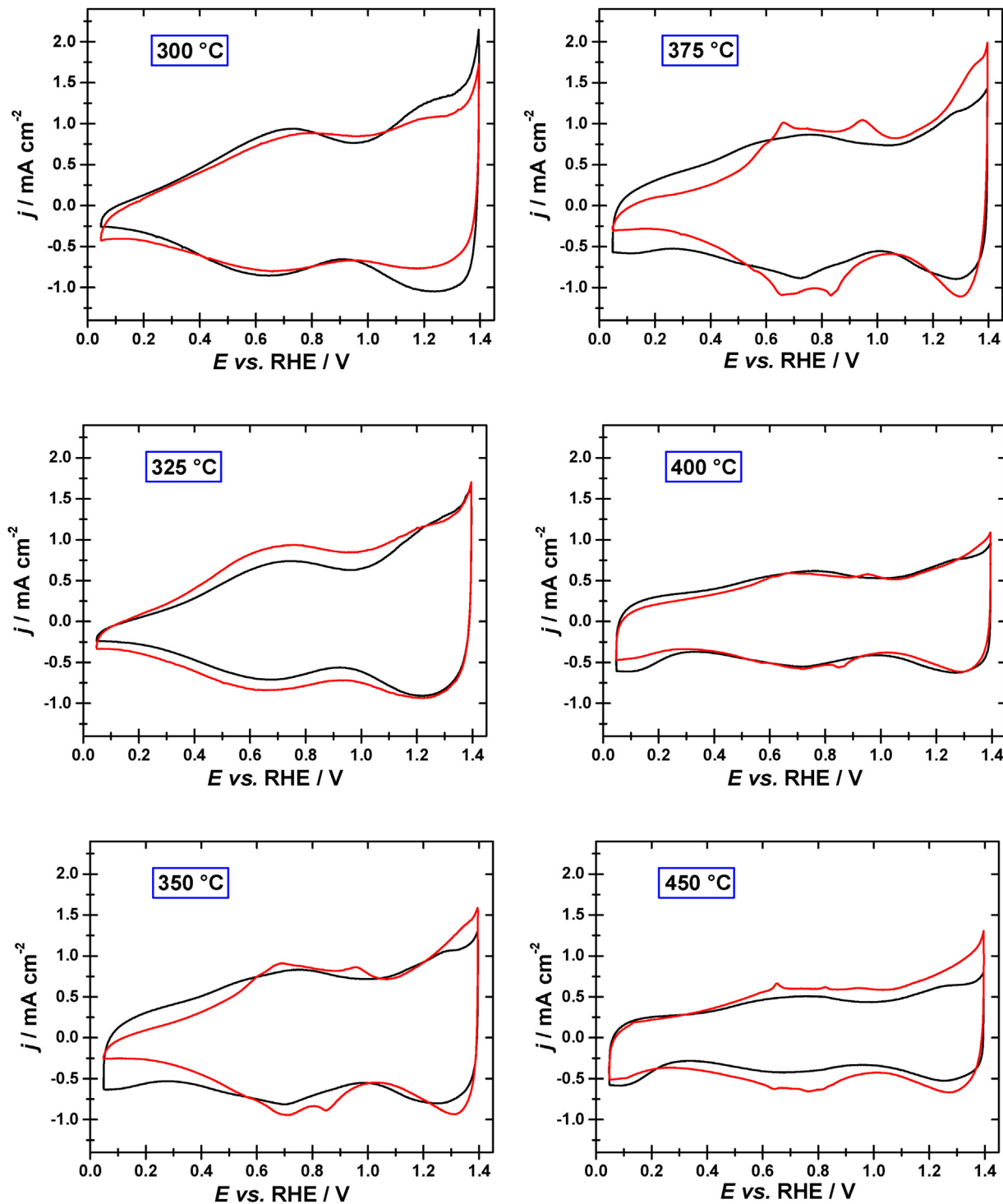


**Fig. 4.** Comparison of the heat treatment atmosphere effect on the RuO<sub>2</sub> CV shape for each annealing temperature. CVs recorded at 20 mV s<sup>-1</sup> in 0.5 M H<sub>2</sub>SO<sub>4</sub> electrolyte under air atmosphere (black line) or nitrogen atmosphere (red line). (For interpretation of the references to colour in this figure legend, the reader is referred to the web version of this article.)

materials annealed at higher temperatures. For materials annealed under nitrogen atmosphere, the trend is first an increase of the specific capacitance value with the increase of the annealing temperature for materials annealed between 300 °C and 325 °C, and then a non-linear decrease for materials annealed at higher temperatures. Barbieri et al. [27] explained that the capacitance values are directly correlated to the electronic and protonic conductivities of the RuO<sub>2</sub> materials. High capacitance values can be obtained either from hydrated particles due to the good accessibility for protons

to the surface, or from materials displaying good electronic conductivity and low hydration level. In our case, the hydration of the materials can explain the high values of the capacitance for materials annealed at low temperatures (300 °C and 325 °C). Indeed, according to the voltammetric measurements, particularly to the shapes of CVs (Fig. 4), the RuO<sub>2</sub> materials seem to be hydrated. In the case of materials annealed under air, the capacitance value continues to increase with the increase of the annealing temperature for materials annealed at 350 °C and 375 °C, whereas for materi-

als annealed under inert atmosphere, it slightly decreases. In the former case the increase of the crystallinity of the RuO<sub>2</sub> particles and the decrease of their hydration level, as shown by the shape of the CVs in Fig. 4, lead to improve the electronic conductivity, whereas in the latter case, the slight decrease of the capacitance value is related to the dehydration process without increase of the crystallinity.

At last, the capacitance values decrease for all materials annealed at higher temperatures, independently on the atmosphere. The loss in capacitance is likely related to the complete dehydration of the RuO<sub>2</sub> nano-particles, the remaining capacitive properties being only due to the electronic conductivity of materials [33]. The slight increase of the capacitance for the samples annealed at 450 °C could be induced by the higher crystallinity of the samples leading to an increase of the electronic conductivity properties of the materials. These observations confirm that the crystallographic structure transition does not occur at the same temperature for samples annealed under air atmosphere as for the materials annealed under inert atmosphere. Considering that the whole mass of RuO<sub>2</sub> materials deposited on the electrode surface takes part in the charging process, the specific capacitance for materials annealed at low temperatures reaches values close to 200 F g<sup>-1</sup>, whereas for materials annealed at high temperatures it reaches values close to 100 F g<sup>-1</sup>, whatever the annealing atmosphere. These specific capacitance values are in good agreement with those reported in the literature for non-supported RuO<sub>2</sub> materials [34–36].

The ratios ( $C(2 \text{ mV s}^{-1})/C(200 \text{ mV s}^{-1})$ ) are reported in Table 2. They are close to 1.2 for all materials, independently of the annealing temperature and atmosphere, which reveals that the modification of the nanoparticle structure does not affect significantly the diffusion of the electro-reactive species towards the active sites. Nevertheless, the values of the ratios are higher for the materials annealed under inert atmosphere than for those annealed under air, which could be due to a higher electroactive surface area in the former case. This observation is in agreement with the presence of sharper peaks superimposed to the redox transitions Ru(III)/Ru(IV) and Ru(IV)/Ru(VI), showing a higher charge transfer rate for the formation of surface hydroxide, *i.e.* higher electroactive surface areas.

For an electrocatalytic application, such as oxygen evolution reaction, the determination of the charges ( $q^*$ ) by integrating the  $I(E)$  curves of the CVs allow estimating the active surface area, *i.e.* the number of active sites in the catalytic layer [37]. The method to calculate  $q^*$  is described in details elsewhere [30]. Briefly, it consists in averaging the anodic and cathodic charges obtained between 0.3 and 1.2 V vs. RHE by the integration of the current intensity for the positive and negative scans of the CVs, respectively. At a very low scan rate, the electro-reactive species can diffuse inside the porosity of the catalytic layer and to react with all the active sites, whereas at high scan rates the reaction can only take place on the most accessible active sites. Ardizzone et al. [38] established two relations (Eqs. (2) and (3)) to calculate the total charges ( $q^*_{\text{Total}}$ ) and the most accessible charges ( $q^*_{\text{Outer}}$ ) when the scan rate values tend to 0 and  $\infty$ , respectively.

$$\frac{1}{q^*} = \frac{1}{q^*_{\text{Outer}}} + C_2 \sqrt{\nu} \quad (2)$$

$$q^* = q^*_{\text{Outer}} + C_1 \frac{1}{\sqrt{\nu}} \quad (3)$$

where  $C_1$  and  $C_2$  are constants,  $\nu$  is the scan rate and  $q^*$  is the average charge calculated for each scan rate  $\nu$ . The  $q^*_{\text{Outer}}$  values are obtained by determining the intercepts of the linear part of the curves for scan rate higher than 20 mV s<sup>-1</sup> (Fig. 5a and c), whereas the  $q^*_{\text{total}}$  values are obtained for scan rate values lower

than 20 mV s<sup>-1</sup> (Fig. 5b and d). Interestingly, all the materials give charge values of same orders of magnitude and the plots of charges versus the scan rate display the same general shape, independently on the annealing atmosphere.

The most accessible charges ( $q^*_{\text{Outer}}$ ) and the total charges ( $q^*_{\text{Total}}$ ) are plotted as a function of the annealing temperature under air and inert atmospheres in Fig. 6a and c, respectively. The values are summarized in Table 3. As can be seen, the charge values are higher for low heat treatment temperature and then, when increasing the temperature over 375 °C the values decrease slightly. For materials annealed under air atmosphere,  $q^*_{\text{Total}}$  and  $q^*_{\text{Outer}}$  values first increase for annealing temperature between 325 °C and 375 °C, as observed for the capacitance, and decrease for higher annealing temperatures. For materials annealed under inert atmosphere,  $q^*_{\text{Total}}$  and  $q^*_{\text{Outer}}$  values are constant for annealing temperature between 325 °C and 375 °C, and decrease for higher annealing temperatures. Once again these changes in  $q^*_{\text{Total}}$  and  $q^*_{\text{Outer}}$  can be related to the hydration and the crystallographic structures of the RuO<sub>2</sub> particles.

The active sites accessibilities,  $A = 100 \times (q^*_{\text{Outer}}/q^*_{\text{Total}})$ , were evaluated (Fig. 6b and d). For materials annealed under air atmosphere, the accessibility values are comprised between 75 and 77% for annealing temperature between 325 °C and 400 °C and then decrease down to 69% for 450 °C. Conversely, for materials annealed under inert atmosphere, the accessibility values first increase from 67% to 75% for annealing temperatures from 300 °C to 375 °C and reach a plateau at 75% for higher temperatures. Materials annealed under inert atmosphere and low temperatures display lower accessibility to active sites than materials annealed under air atmosphere, which can be explained as a consequence of the higher hydration of the nanoparticles. But, for higher annealing temperatures, from ca. 375 °C, when the water content in nanoparticles decreases and the crystalline structure appears, the accessibility becomes close to that determined for materials annealed under air atmosphere. This observation is consistent with the fact that the annealing process under nitrogen atmosphere leads to delay the formation of the rutile crystalline structure and the dehydration of the RuO<sub>2</sub> particles. At last, generally speaking, all accessibility values are higher than 67%, so that the majority of the active sites are accessible regardless the annealing temperature and atmosphere.

The electrocatalytic properties of RuO<sub>2</sub> materials toward the oxygen evolution reaction (OER) have been determined by recording the anodic polarization curves between 1.0 V and 1.8 V vs. RHE (Fig. 7a and b). All current intensities were normalized to the geometric surface area of the working electrode loaded with the same amount of catalytic materials. All catalysts show an OER onset potential close to 1.45 V vs. RHE and gave abundant bubbling at higher potentials. The polarization curves normalized to the total charges are depicted in the inset of Fig. 7a and b in order to evaluate the electrocatalytic activities per active site. With this normalization, it can be seen that the electrocatalytic performances at high potentials increase gradually when increasing the annealing temperature. For materials annealed at 300 °C, the onset potential of OER is slightly lower than that obtained for higher annealing temperatures, which can be linked to the low crystallinity of the materials and to their high hydration level, but activity decreases drastically for high potentials. Intermediate activities of same order of magnitude are obtained for materials annealed at 350 °C and 375 °C, and at last higher activities are obtained for materials annealed at 400 °C and 450 °C. It is likely that the intrinsic efficiency of active sites is principally linked to the crystallinity of the RuO<sub>2</sub> particles. Indeed, the IM-450-Air and IM-450-N<sub>2</sub> samples, which present the highest crystallinity as determined from XRD and observed from TEM measurements, also lead to the highest electrocatalytic performances although these materials display

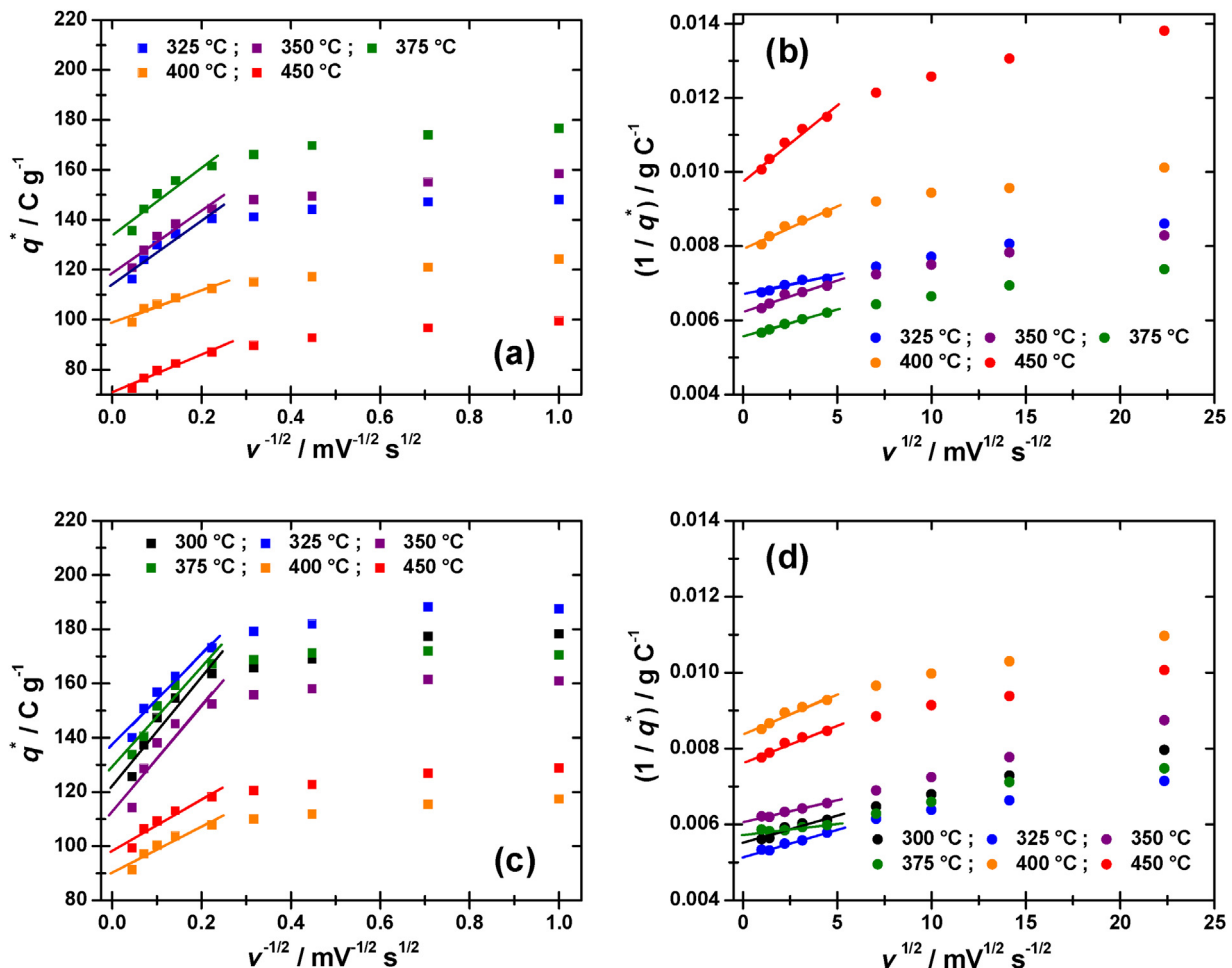


**Fig. 5.** Voltammetric charges versus the scan rate for RuO<sub>2</sub> materials (a, b) annealed under air and (c, d) annealed under nitrogen atmosphere. (a, c) plots for the extrapolation of the most accessible charges ( $q^*_{\text{outer}}$ ) and (b and d) plots for the extrapolation of the total charges ( $q^*_{\text{total}}$ ).

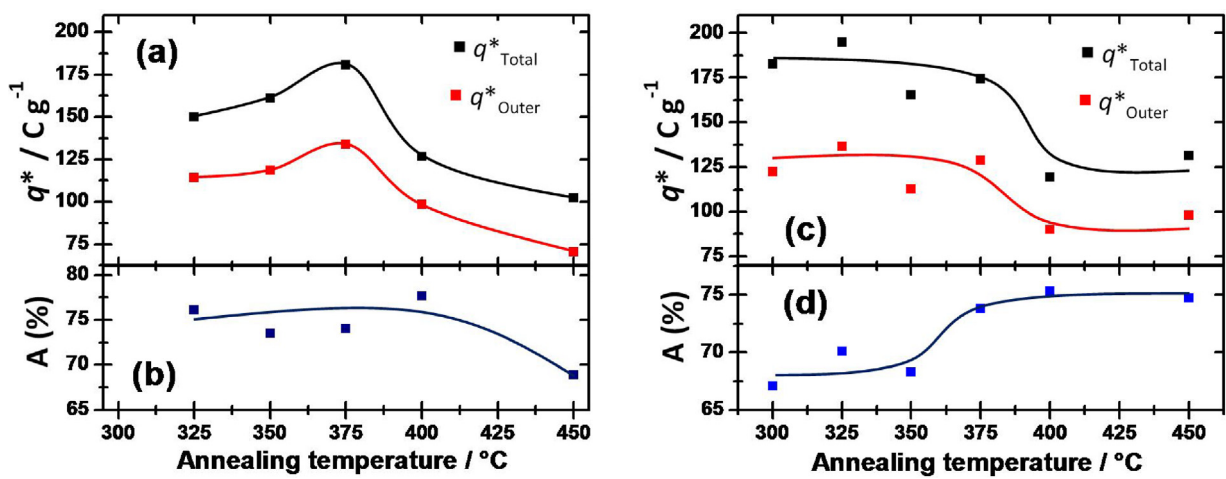


**Fig. 6.** (a, c) Total charges ( $q^*_{\text{total}}$ ) and most accessible charges ( $q^*_{\text{outer}}$ ), and (b, d) active site accessibility ( $A = 100 \times (q^*_{\text{outer}}/q^*_{\text{total}})$ ) for RuO<sub>2</sub> materials as a function of the annealing temperature (a, b) under air atmosphere and (c, d) under nitrogen atmosphere.

lower current densities referred to the active sites than the other RuO<sub>2</sub> samples.

In order to determine possible effects of the annealing atmosphere, the polarization curves of materials annealed under air and under inert atmospheres are compared for each annealing temperature in Fig. 8. The IM-300-N<sub>2</sub> catalyst reaches a maximum

current density at 1.57 V vs. RHE (ca. 50 mA cm<sup>-2</sup>) and then the current density decreases drastically down to ca. 2 mA cm<sup>-2</sup> for higher potentials. Moreover, a shoulder is clearly distinguishable at the same potential (1.57 V vs. RHE) for IM-325-N<sub>2</sub>, and the current density continues to increase for higher potentials. The polarization curve recorded on the IM-300-Air catalyst displays the same

**Table 3**

Electrochemical data obtained for the RuO<sub>2</sub> materials synthesized by the Instant Method at different annealing temperatures ( $q^*_{\text{total}}$  = total voltammetric charge,  $q^*_{\text{outer}}$  = most accessible charge, A = accessibility, b = Tafel slope and  $j_0$  = exchange current density for the OER).

	$q^*_{\text{total}}/\text{C g}^{-1}$		$q^*_{\text{outer}}/\text{C g}^{-1}$		A/% ( $q^*_{\text{outer}}/q^*_{\text{total}}$ )		b (mV dec <sup>-1</sup> )		$j_0$ (mA cm <sup>-2</sup> )	
	Air	N <sub>2</sub>	Air	N <sub>2</sub>	Air	N <sub>2</sub>	Air	N <sub>2</sub>	Air	N <sub>2</sub>
IM-300	n.d.	182.5	n.d.	122.3	n.d.	67.0	51.2	49.7	$1.1 \cdot 10^{-4}$	$1.0 \cdot 10^{-4}$
IM-325	150.2	194.9	114.2	136.7	76.1	70.1	59.7	54.7	$2.9 \cdot 10^{-4}$	$1.6 \cdot 10^{-4}$
IM-350	161.0	165.3	118.4	112.9	73.5	68.3	52.8	53.8	$8.9 \cdot 10^{-5}$	$1.2 \cdot 10^{-4}$
IM-375	180.8	174.5	133.9	128.8	74.0	73.8	52.6	56.4	$6.1 \cdot 10^{-5}$	$2.4 \cdot 10^{-4}$
IM-400	126.6	119.6	98.3	90.1	77.6	75.3	46.4	49.6	$1.5 \cdot 10^{-5}$	$3.3 \cdot 10^{-5}$
IM-450	102.5	131.4	70.6	98.2	68.9	74.7	44.9	51.3	$8.5 \cdot 10^{-6}$	$6.1 \cdot 10^{-5}$

n.d.: not determined.

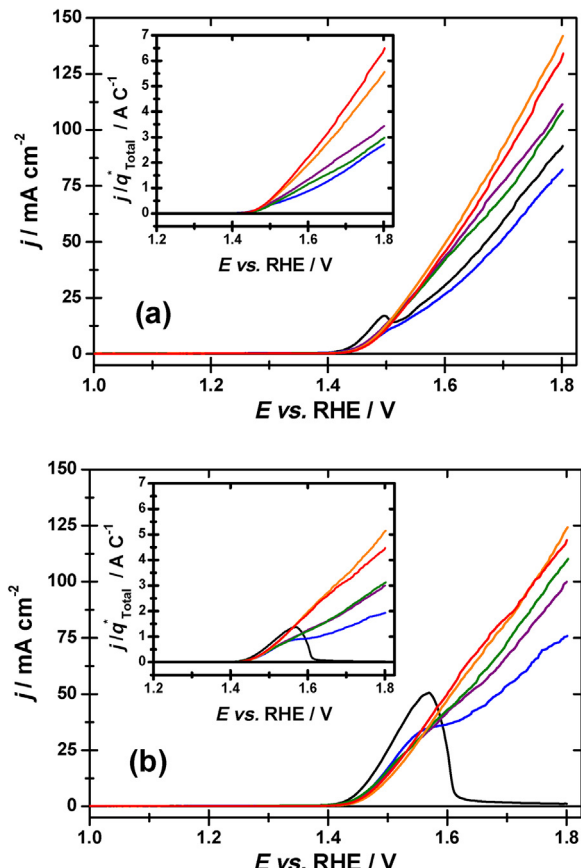


**Fig. 7.** Polarization curves recorded at 5 mV s<sup>-1</sup> in 0.5 M H<sub>2</sub>SO<sub>4</sub> supporting electrolyte of RuO<sub>2</sub> electrodes obtained for all annealing temperature (a) under air atmosphere and (b) under nitrogen atmosphere. Current densities are normalized to the geometric surface area of the electrode. Inset: polarization curves with the current densities normalized to the total charges ( $q^*_{\text{total}}$ ). Black lines: annealing at 300 °C; blue lines: annealing at 325 °C; purple lines: annealing at 350 °C; green lines: annealing at 375 °C; yellow lines: annealing at 400 °C; and red lines: annealing at 450 °C. (For interpretation of the references to colour in this figure legend, the reader is referred to the web version of this article.)

behaviour as that on IM-300-N<sub>2</sub> since the OER onset potential occurs at ca. 1.5 V, where a current density peak is reached. For higher potentials, the current density starts to decrease and then increases almost exponentially. Again, the current density peak observed at ca. 1.5 V on the IM-300-Air catalyst becomes a shoulder in the case of the IM-325-Air catalyst. Similar results to those obtained for IM-300-N<sub>2</sub> are reported in the literature for hydrous or non-crystalline ruthenium oxides [20,39]. However the involved reactions and mechanisms are not clearly defined. Since the formation of bubbles was observed at the electrode surface, the anodic currents at low overpotentials are attributed to the OER process for all catalysts obtained at annealing temperatures of 300 and

325 °C. The total or partial passivation of the electrode materials for higher potentials is not clearly understood but could come from oxide material instabilities induced by the hydration level, the size and the low crystallinity of the ruthenium oxide particles. The observations of a peak for IM-300-N<sub>2</sub> and only a shoulder for IM-325-N<sub>2</sub> could indicate that the OER process occurs firstly from the water molecules included in the crystallographic structure of RuO<sub>2</sub>. The presence of water molecules at the vicinity of active sites could allow the reaction to take place at lower potentials than those with pure crystalline materials. Furthermore, the water oxidation process in the crystal lattice could induce changes in the crystallographic structure and confer new properties to the materials, which could explain the passivation process for IM-300-N<sub>2</sub>. When the annealing temperature is increased, the hydration level of particles is decreased, therefore the modifications induced by the water oxidation process in the crystal lattice are minimized and the OER process can continue at higher potentials.

For materials annealed at temperature higher than 350 °C, the polarization curves obtained are characteristic of the classical OER process on RuO<sub>2</sub> materials, with an onset potential of ca. 1.42 V vs. RHE and anodic current densities increasing steadily. Although the numbers of active sites are different, the current density recorded for a given potential higher than 1.6 V vs. RHE increases with the annealing temperature of materials, indicating that the efficiency of the catalysts for the reaction taking place on their surface is directly correlated to the crystallinity of the oxide materials. The best performances are obtained for RuO<sub>2</sub> materials annealed at 400 °C under air and 450 °C under nitrogen and are very close for both annealing atmospheres. It is worth to note that higher performances are reached for the crystallite size of 18.2 nm in both case, which could also indicate a size effect in the catalytic behavior.

From the experimental polarization curves, the Tafel plots have been determined and are shown in Fig. 9a and b. The low potential region corresponds to residual capacitive currents. Then the plots in the potential region between 1.4 and 1.5 V vs. RHE are quasi linear. In this low overpotential range, it can be assumed that ohmic drop has nearly no effect on the j-E curve shape [40,41], so that the Tafel slopes can be determined in this potential range, where  $j < 20 \text{ mA cm}^{-2}$ . The Tafel slopes (b) will allow determining the rate determining step of the OER mechanism and the exchange current densities ( $j_0$ ) related to the kinetics of the OER. The values are summarized in Table 3. For all materials, the values of the exchange current density indicate that the OER is a slow process ( $j_0 < 10^{-4} \text{ A cm}^{-2}$ ). Moreover, the  $j_0$  values decrease by ca. one order of magnitude when the annealing temperature is increased. This observation could be explained by the fact that in the case of hydrated particles, the water molecules trapped in the crystal lattice are more easily oxidized. Due to the presence of these trapped water molecules at the vicinity of the active sites, their oxidation is slightly faster than that for molecules present in the bulk of electrolyte. Thus, for crystalline particles, which present also very low hydration levels, the OER process takes place more slowly. Conversely, taking into account the shape of the polarization curves,

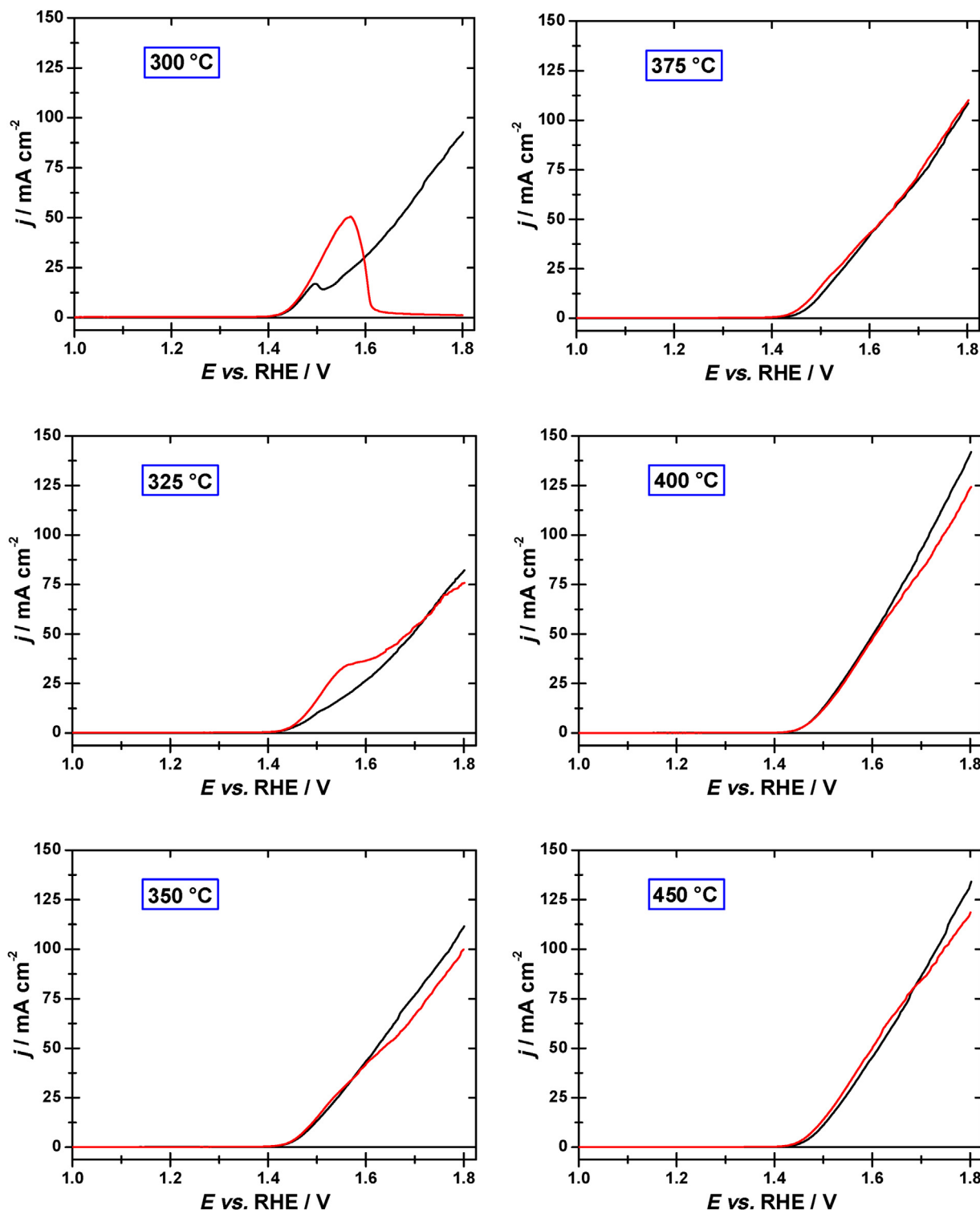


**Fig. 8.** Comparison of the polarization curves recorded at 5 mV s<sup>-1</sup> in 0.5 M H<sub>2</sub>SO<sub>4</sub> electrolyte of materials annealed in different atmosphere (black lines: air atmosphere, red lines: nitrogen atmosphere) at each annealing temperature. (For interpretation of the references to colour in this figure legend, the reader is referred to the web version of this article.)

higher electrocatalytic performances for the OER are obtained at high potentials, which can be linked to the reaction mechanism occurring at the RuO<sub>2</sub> particle surface.

Due to the complex reaction of water oxidation involving the transfer of 4-electrons, several mechanisms were considered with different rate-determining steps [42]. The following mechanism was proposed for the OER in acid medium on active oxide elec-

trodes [43] and starting from the water adsorption on the active site (S) with charge transfer leading to an intermediate hydroxyl species:



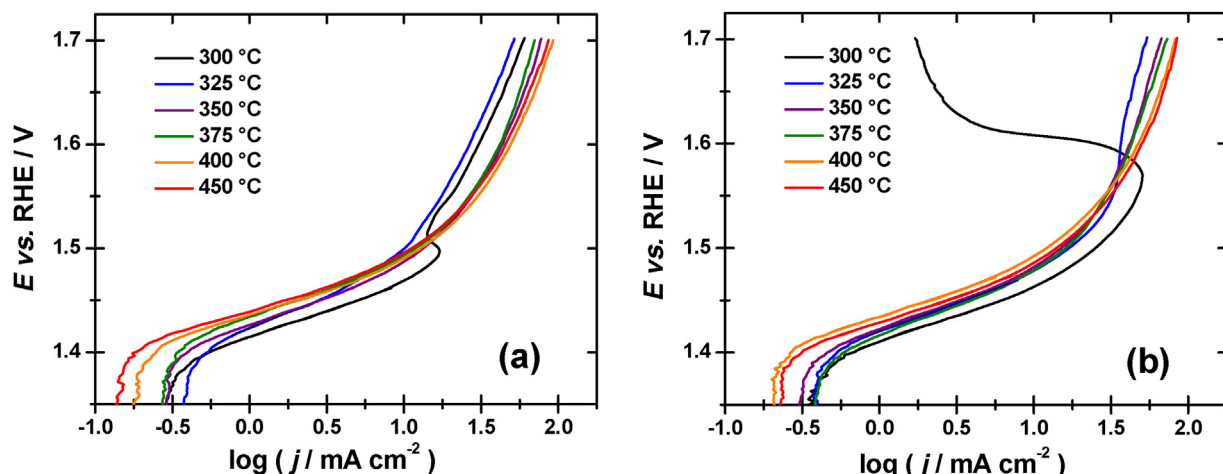


**Fig. 9.** Tafel curves obtained from OER polarization measurements for RuO<sub>2</sub> electrodes obtained at all annealing temperature (a) under air atmosphere (b) and under nitrogen atmosphere.

the second step can occur through an electrochemical path with a second electron transfer which consists in the deprotonation of the intermediate species leading to a surface oxide species:



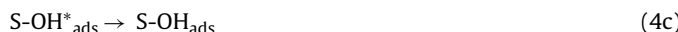
However, an alternative step, *i.e.* a recombination step of an oxide, can take place in parallel due to the bond strength of the intermediate species to the active site:



and finally, the combination of the two intermediate species leads to the formation of O<sub>2</sub>:



It has been shown for this mechanism that the Tafel slopes values should be 120 mV dec<sup>-1</sup> for a rate determining step described by Eq. (4a), 40 mV dec<sup>-1</sup> for a rate determining step described by Eq. (5a) (this value can be slightly different due to the intervention of the step described by Eq. (5b) leading to values close to 30 mV dec<sup>-1</sup>), and finally 15 mV dec<sup>-1</sup> for a rate determining step described by Eq. (6) [43–45]. However, alternative steps can take place depending on the bond strength of the intermediate species to the active sites which can differ with the catalytic layer composition, and thus can lead to different Tafel slope values. Thus, the step described in Eq. (4a) can be dissociated into two reactions:



where the intermediate species S-OH<sub>ads</sub> and S-OH<sup>\*</sup><sub>ads</sub> have the same chemical structure but different bond strengths depending on the active site nature. Both steps can occur alternatively or in parallel, and the Tafel slope value is then 60 mV dec<sup>-1</sup> if they are the rate determining step. Whatever the atmosphere or the temperature of the heat treatment, the Tafel slope values do not differ much, and are comprised between 45 and 60 mV dec<sup>-1</sup> (Fig. 10). Although slightly higher, the obtained values are in agreement with those observed in the literature at room temperature for the oxygen evolution process with ruthenium oxide based electrodes [44,46,47]. This small discrepancy can be due to the electrode preparation which could lead to the formation of a compact oxide film [48] or to the hydration of the particles which can act as a barrier for the electron hopping process. The rate determining step is the same for all catalysts, being the second charge transfer step described in Eq.

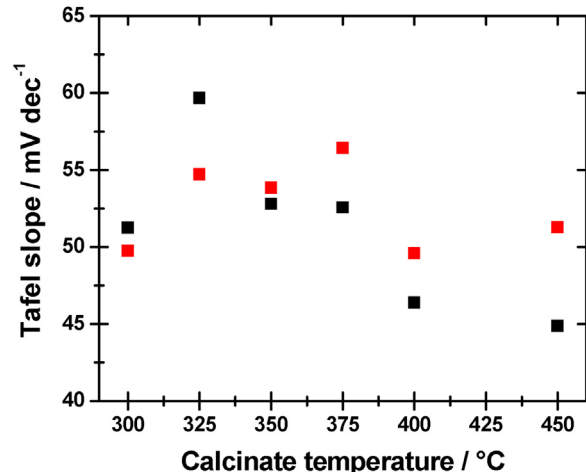


**Fig. 10.** Tafel slopes values measured at low overpotential for RuO<sub>2</sub> electrocatalysts synthesized by the Instant Method as a function of the annealing temperature under air atmosphere (black) and under nitrogen atmosphere (red). (For interpretation of the references to colour in this figure legend, the reader is referred to the web version of this article.)

(5a). This one seems to be more related to the nature of the electrocatalytic material (RuO<sub>2</sub>) than to the annealing temperature and/or atmosphere.

#### 4. Conclusion

In this work, the syntheses of crystalline RuO<sub>2</sub> materials have been carried out using the Instant Method followed by an annealing step under air or nitrogen atmospheres. The physicochemical and electrochemical characterizations have shown that the main effect of the annealing atmosphere is the modification of the transition temperature from an amorphous hydrated phase of ruthenium oxide to a crystalline phase (at ca. 300 °C under air and ca. 350 °C under nitrogen). But, whatever the annealing temperature and atmosphere, the values of the capacitances, of the charges involved in the CVs and of the OER Tafel slopes, are always very close, which indicates that these synthesis parameters have a few influence on the material properties.

It has been shown that higher catalytic activities towards the OER were obtained at high overpotentials ( $E > 1.6 \text{ V vs. RHE}$ ) in both cases after annealing at high temperatures, *i.e.* 400 °C to 450 °C. It was also shown that the activity of the catalysts annealed at 400 °C

or 450 °C is independent of the annealing atmosphere, and that the same performances as those of the state-of-the-art ruthenium oxide catalysts were reached. This is an important result which confirms that metal oxide syntheses can be performed under inert atmosphere, allowing further one-pot syntheses of supported catalysts on different kinds of electron-conductive supports. However, higher activity in terms of exchange current density  $j_0$  was obtained at low OER overpotentials ( $E < 1.5$  V vs. RHE) for hydrated ruthenium oxide compounds; this study allowed us demonstrating for the first time to our knowledge that the improvement of the water oxidation kinetics is related to the oxidation of water molecules trapped in the ruthenium oxide lattice.

Therefore, the tuning of the annealing temperature is of great importance in order to obtain the best balance between the hydration level and the crystallinity of materials, and further the highest catalytic activity towards OER.

## Acknowledgements

The authors greatly acknowledge the CNRS Research Grouping HySpaC (GDR n°3652) and the Institute of Chemistry of the “Centre National de la Recherche Scientifique” (CNRS) for supporting this work. One of us (TA) also acknowledges Roger Milly at Soprono for providing him a postdoctoral stay at the IC2MP.

## References

- [1] S. Dunn, Hydrogen futures: toward a sustainable energy system, *Int. J. Hydrogen Energy* 27 (2002) 235–264.
- [2] A.M. Omer, Energy, environment and sustainable development, *Renew. Sustain. Energy Rev.* 12 (2008) 2265–2300.
- [3] J.D. Holladay, J. Hu, D.L. King, Y. Wang, An overview of hydrogen production technologies, *Catal. Today* 139 (2009) 244–260.
- [4] S. Trasatti, Electrocatalysis in the anodic evolution of oxygen and chlorine, *Electrochim. Acta* 29 (1984) 1503–1512.
- [5] D.B. Rogers, R.D. Shannon, A.W. Sleight, J.L. Gillson, Crystal chemistry of metal dioxides with rutile-related structures, *Inorg. Chem.* 8 (1969) 841–849.
- [6] M.H. Miles, M.A. Thomason, Periodic variations of overvoltages for water electrolysis in acid solutions from cyclic voltammetric studies, *J. Electrochem. Soc.* 123 (1976) 1459–1461.
- [7] A. Di Blasi, C. D'Urso, V. Baglio, V. Antonucci, A.S. Aricò, R. Ornelas, F. Matteucci, G. Orozco, D. Beltran, Y. Meas, L.G. Arriaga, Preparation and evaluation of RuO<sub>2</sub>–IrO<sub>2</sub>, IrO<sub>2</sub>–Pt and IrO<sub>2</sub>–Ta<sub>2</sub>O<sub>5</sub> catalysts for the oxygen evolution reaction in an SPE electrolyzer, *J. Appl. Electrochem.* 39 (2008) 191–196.
- [8] Y. Murakami, S. Tsuchiya, K. Yahikozawa, Y. Takasu, Preparation of ultrafine RuO<sub>2</sub> and IrO<sub>2</sub> particles by a sol-gel process, *J. Mater. Sci. Lett.* 13 (1994) 1773–1774.
- [9] A.T. Marshall, R.G. Haverkamp, Electrocatalytic activity of IrO<sub>2</sub>–RuO<sub>2</sub> supported on Sb-doped SnO<sub>2</sub> nanoparticles, *Electrochim. Acta* 55 (2010) 1978–1984.
- [10] G. Li, H. Yu, W. Song, X. Wang, Y. Li, Z. Shao, B. Yi, Zeolite-templated Ir<sub>x</sub>Ru<sub>1-x</sub>O<sub>2</sub> electrocatalysts for oxygen evolution reaction in solid polymer electrolyte water electrolyzers, *Int. J. Hydrogen Energy* 37 (2012) 16786–16794.
- [11] X. Wu, K. Scott, RuO<sub>2</sub> supported on Sb-doped SnO<sub>2</sub> nanoparticles for polymer electrolyte membrane water electrolyzers, *Int. J. Hydrogen Energy* 36 (2011) 5806–5810.
- [12] J.C. Cruz, S. Rivas, D. Beltran, Y. Meas, R. Ornelas, G. Osorio-Monreal, L. Ortiz-Frade, J. Ledesma-Garcia, L.G. Arriaga, Synthesis and evaluation of ATO as a support for Pt–IrO<sub>2</sub> in a unitized regenerative fuel cell, *Int. J. Hydrogen Energy* 37 (2012) 13522–13528.
- [13] S. Siracusano, V. Baglio, C. D'Urso, V. Antonucci, A.S. Aricò, Preparation and characterization of titanium suboxides as conductive supports of IrO<sub>2</sub> electrocatalysts for application in SPE electrolyzers, *Electrochim. Acta* 54 (2009) 6292–6299.
- [14] L. Ma, S. Sui, Y. Zhai, Preparation and characterization of Ir/TiC catalyst for oxygen evolution, *J. Power Sources* 177 (2008) 470–477.
- [15] S.-Y. Huang, P. Ganeshan, H.-Y. Jung, B.N. Popov, Development of supported bifunctional oxygen electrocatalysts and corrosion-resistant gas diffusion layer for unitized regenerative fuel cell applications, *J. Power Sources* 198 (2012) 23–29.
- [16] G. García, M. Roca-Ayats, A. Lillo, J.L. Galante, M.A. Pena, M.V. Martínez-Huerta, Catalyst support effects at the oxygen electrode of unitized regenerative fuel cells, *Catal. Today* 210 (2013) 67–74.
- [17] J. Ma, M. Wu, Y. Du, S. Chen, G. Li, J. Hu, Synthesis of nanocrystalline titanium carbide with a new convenient route at low temperature and its thermal stability, *Mater. Sci. Eng. B* 153 (2008) 96–99.
- [18] Y. Chen, H. Zhang, D. Ma, J. Ma, H. Ye, G. Qian, Y. Ye, Synthesis thermal stability, and photocatalytic activity of nanocrystalline titanium carbide, *Mater. Res. Bull.* 46 (2011) 1800–1803.
- [19] J. Ma, M. Wu, Y. Du, S. Chen, G. Li, J. Hu, Synthesis of nanocrystalline titanium nitride at low temperature and its thermal stability, *J. Alloys Compd.* 476 (2009) 603–605.
- [20] A. Devadas, S. Baranton, T. Napporn, C. Coutanceau, Tailoring of RuO<sub>2</sub> nanoparticles by microwave assisted “Instant method” for energy storage applications, *J. Power Sources* 196 (2011) 4044–4053.
- [21] J.C. Cruz, V. Baglio, S. Siracusano, V. Antonucci, A.S. Aricò, R. Ornelas, L. Ortiz-Frade, G. Osorio-Monreal, S.M. Durón-Torres, L.G. Arriaga, Preparation and characterization of RuO<sub>2</sub> catalysts for oxygen evolution in a solid polymer electrolyte, *Int. J. Electrochem. Sci.* 6 (2011) 6607–6619.
- [22] E. Tsuji, A. Imanishi, K.-I. Fukui, Y. Nakato, Electrocatalytic activity of amorphous RuO<sub>2</sub> electrode for oxygen evolution in an aqueous solution, *Electrochim. Acta* 56 (2011) 2009–2016.
- [23] C. Sassoye, G. Muller, D.P. Debecker, A. Karelovic, S. Cassaignon, C. Pizarro, P. Ruiz, C. Sanchez, A sustainable aqueous route to highly stable suspensions of monodispersed nano ruthenia, *Green Chem.* 13 (2011) 3230–3237.
- [24] T. Audichon, E. Mayousse, T.W. Napporn, C. Morais, C. Comminges, K.B. Kokoh, Elaboration and characterization of ruthenium nano-oxides for the oxygen evolution reaction in a Proton Exchange Membrane Water Electrolyzer supplied by a solar profile, *Electrochim. Acta* 132 (2014) 284–291.
- [25] V. Natarajan, S. Basu, K. Scott, Effect of treatment temperature on the performance of RuO<sub>2</sub> anode electrocatalyst for high temperature proton exchange membrane water electrolyzers, *Int. J. Hydrogen Energy* 38 (2013) 16623–16630.
- [26] K.-H. Chang, C.-C. Hu, C.-Y. Chou, Textural and capacitive characteristics of hydrothermally derived RuO<sub>2</sub>·xH<sub>2</sub>O nanocrystallites: independent control of crystal size and water content, *Chem. Mater.* 19 (2007) 2112–2119.
- [27] O. Barbieri, M. Hahn, A. Foelske, R. Kötz, Effect of electronic resistance and water content on the performance of RuO<sub>2</sub> for supercapacitors, *J. Electrochem. Soc.* 153 (2006) A2049–A2054.
- [28] R. Kötz, S. Stucki, Stabilisation of RuO<sub>2</sub> by IrO<sub>2</sub> for anodic oxygen evolution in acid media, *Electrochim. Acta* 31 (1986) 1311–1316.
- [29] V.A. Saveleva, L. Wang, W. Luo, S. Zafeiratos, C. Ulhaq-Bouillet, A.S. Gago, K.A. Friedrich, E.R. Savinova, Uncovering the stabilization mechanism in bimetallic ruthenium–iridium anodes for proton exchange membrane electrolyzers, *J. Phys. Chem. Lett.* 7 (2016) 3240–3245.
- [30] C.-C. Hu, K.-H. Chang, Cyclic voltammetric deposition of hydrous ruthenium oxide for electrochemical capacitors: effects of codepositing iridium oxide, *Electrochim. Acta* 45 (2000) 2685–2696.
- [31] T. Hepel, F.H. Pollak, Effect of crystallographic orientation of single-crystal RuO<sub>2</sub> electrodes on the hydrogen adsorption reactions, *Solid State Sci. Technol.* 131 (1984) 2094–2100.
- [32] T. Audichon, B. Guenot, S. Baranton, M. Cretin, C. Lamy, C. Coutanceau, Preparation and characterization of supported Ru<sub>x</sub>Ir<sub>(1-x)</sub>O<sub>2</sub> nano-oxides using a modified polyol synthesis assisted by microwave activation for energy storage applications, *Appl. Catal. B* 200 (2017) 493–502.
- [33] J.P. Zheng, Y. Xin, Characterization of RuO<sub>2</sub>·xH<sub>2</sub>O with various water contents, *J. Power Sources* 110 (2002) 86–90.
- [34] K. Juodkazis, J. Juodkazytė, V. Šukienė, A. Grigucevičienė, A. Selskis, On the charge storage mechanism at RuO<sub>2</sub>/0.5 M H<sub>2</sub>SO<sub>4</sub> interface, *J. Solid State Electrochem.* 12 (2008) 1399–1404.
- [35] J.P. Zheng, T.R. Jow, A new charge storage mechanism for electrochemical capacitors, *J. Electrochim. Soc.* 142 (1995) L6–L8.
- [36] W. Sugimoto, K. Yokoshima, Y. Murakami, Y. Takasu, Charge storage mechanism of nanostructured anhydrous and hydrous ruthenium-based oxides, *Electrochim. Acta* 52 (2006) 1742–1748.
- [37] S. Ardizzone, S. Trasatti, Interfacial properties of oxides with technological impact in electrochemistry, *Adv. Colloid Interface Sci.* 64 (1996) 173–251.
- [38] S. Ardizzone, G. Fregonara, S. Trasatti, “Inner” and “Outer” active surface of RuO<sub>2</sub> electrodes, *Electrochim. Acta* 35 (1990) 263–267.
- [39] T. Audichon, T.W. Napporn, C. Canaff, C. Morais, C. Comminges, K.B. Kokoh, IrO<sub>2</sub> coated on RuO<sub>2</sub> as efficient and stable electroactive nanocatalysts for electrochemical water splitting, *J. Phys. Chem. C* 120 (2016) 2562–2573.
- [40] L.-E. Owe, M. Tsypkin, K.S. Wallwork, R.G. Haverkamp, S. Sunde, Iridium–ruthenium single phase mixed oxides for oxygen evolution: composition dependence of electrocatalytic activity, *Electrochim. Acta* 70 (2012) 158–164.
- [41] M.H.P. Santana, L.A. De Faria, Oxygen and chlorine evolution on RuO<sub>2</sub>·TiO<sub>2</sub>·CeO<sub>2</sub>·Nb<sub>2</sub>O<sub>5</sub> mixed oxide electrodes, *Electrochim. Acta* 51 (2006) 3578–3585.
- [42] Y. Matsumoto, E. Sato, Electrocatalytic properties of transition metal oxides for oxygen evolution reaction, *Mater. Chem. Phys.* 14 (1986) 397–426.
- [43] E. Antolini, Iridium as catalyst and cocatalyst for oxygen evolution/reduction in acidic polymer electrolyte membrane electrolyzers and fuel cells, *ACS Catal.* 4 (2014) 1426–1440.
- [44] L.M. Da Silva, J.F.C. Boodts, L.A. De Faria, Oxygen evolution at RuO<sub>2(1-x)</sub>·Co<sub>3</sub>O<sub>4(1-x)</sub> electrodes from acid solution, *Electrochim. Acta* 46 (2001) 1369–1375.
- [45] L.A. De Faria, J.F.C. Boodts, S. Trasatti, Electrocatalytic properties of ternary oxide mixtures of composition Ru<sub>0.3</sub>Ti<sub>(0.7-x)</sub>Ce<sub>x</sub>O<sub>2</sub>: oxygen evolution from acidic solution, *J. Appl. Electrochem.* 26 (1996) 1195–1199.

- [46] X. Wu, J. Tayal, S. Basu, K. Scott, Nano-crystalline  $\text{Ru}_x\text{Sn}_{1-x}\text{O}_2$  powder catalysts for oxygen evolution reaction in proton exchange membrane water electrolyzers, *Int. J. Hydrogen Energy* 36 (2011) 14796–14804.
- [47] K.A. Stoerzinger, L. Qiao, M.D. Biegalski, Y. Shao-Horn, Orientation-dependent oxygen evolution activities of rutile  $\text{IrO}_2$  and  $\text{RuO}_2$ , *J. Phys. Chem. Lett.* 5 (2014) 1636–1641.
- [48] G. Lodi, E. Sivieri, A. De Battisti, S. Trasatti, Ruthenium dioxide-based film electrodes: III. Effect of chemical composition and surface morphology on oxygen evolution in acid solutions, *J. Appl. Electrochem.* 8 (1978) 135–143.